

This is the accepted manuscript made available via CHORUS. The article has been published as:

Importance of orbital fluctuations for the magnetic dynamics in the heavy-fermion compound SmB_{6}

Christopher N. Singh and Wei-Cheng Lee

Phys. Rev. B **97**, 241107 — Published 14 June 2018

DOI: [10.1103/PhysRevB.97.241107](https://doi.org/10.1103/PhysRevB.97.241107)

Importance of orbital fluctuations on magnetic dynamics in heavy fermion SmB₆

Christopher N. Singh^{*} and Wei-Cheng Lee[†]

Binghamton University Department of Physics Applied Physics and Astronomy

(Dated: June 4, 2018)

The emergent dynamical processes associated with magnetic excitations in heavy fermion SmB₆ are investigated. By imposing multi-orbital interactions on a first principles model, we find the interplay between spin and orbital fluctuations in the f manifold is highly sensitive to local correlations. The magnetic phase diagram constructed at zero temperature reveals quantum critical features with the existence of several competing phases. Within the random phase approximation, we perform a comprehensive study of the spin-spin correlation function, and our results agree with neutron scattering experiments. Spectral weight analysis shows the low energy spin excitations are selectively accompanied by orbital fluctuations, indicating a non-trivial entanglement between the spin and orbital degree of freedom driven by relativistic couplings.

Introduction – While the possibility that SmB₆ is topologically non-trivial has driven many recent efforts^{1–12}, an equally relevant aspect of this material has been brought to light through the lens of inelastic magnetic neutron scattering (INS). Specifically, the temperature activated¹³ dynamical magnetic response signatures observed deep within the insulating state are not traditional magnons, show a high degree of momentum space anisotropy, and have been attributed to correlation driven exciton^{14–16} modes. The narrow gap, strong Coulomb interaction, and residual specific heat give exciton-type modes considerable plausibility in the context of this system¹⁷, and identifying the extent to which these excitations contribute to the low energy transport properties, as well as the interplay between correlation and topology is crucial in understanding SmB₆. In fact, it is well known in the heavy fermions that the Coulomb interaction, lattice geometry, and spin orientation are essential in spawning exotic phenomena, however fair treatment of the multi-orbital nature is often hindered by an exponential growth in complexity. It is precisely this interplay of competing energy scales and many degrees of freedom that invoke the striking electronic properties, yet in spite of this, a multi-orbital, first principles study of the magnetic dynamics in SmB₆ is still lacking.

We address this gap with a realistic model based on complementing density functional theory (DFT) with the generalized random phase approximation (GRPA). This is achieved by projecting the relativistic eigenstates of the Kohn-Sham equations onto Wannier functions, and imposing the multi-orbital Hubbard-Kanamori interaction onto these maximally localized orbitals. This approach treats the spin-orbit coupling, multi-orbital Coulomb interaction, and bandstructure effects on equal footing. Quantum critical features are found at zero temperature with several nearby magnetic phases. In the normal state at finite temperature, the low-energy spin excitations are shown to be tightly coupled to orbital exchange processes through the large spin-orbit coupling, and a number of important features observed in the INS experiments naturally emerge with this approach.

Model – Motivated to capture hybridization effects between localized Sm $4f$ moments, and itinerant Sm $5d$

states, we employ a relativistic multi-orbital Hamiltonian as

$$H = H_t + H_{int} \quad (1)$$

where H_t is given by

$$H_t = \frac{1}{2} \sum_{ij\alpha\beta\sigma} (t_{ij}^{\alpha\beta} - 2\mu\delta_{ij}\delta_{\alpha\beta}) c_{i\alpha\sigma}^\dagger c_{j\beta\sigma} \quad (2)$$

Here the fermion operators create (destroy) particles at site i (j), with orbital character α (β) and spin σ . Symmetry considerations and the spin-orbit interaction dictate the Wannier basis is chosen as spinors of the Sm d - eg states and the full Sm f level multiplet¹⁸. In this way, contained within H_t is the fully relativistic ab initio information pertaining to the entirety of the d - f hybridization, as well as f level character in the vicinity of the Fermi energy. This approach has the advantage of treating the f manifold relativistically in contrast to previous studies¹⁵, and is known to be sufficient in producing the hybridization gap¹⁹.

$$\begin{aligned} H_{int} = & \frac{U}{2} \sum_{i\alpha\sigma} n_{i\alpha\sigma} n_{i\alpha\sigma} \\ & + \sum_{i,\alpha<\beta,\sigma} \{ (U - 2J) n_{i\alpha\sigma} n_{i\beta\sigma} + (U - 3J) n_{i\alpha\sigma} n_{i\beta\sigma} \\ & + J (c_{i\alpha\sigma}^\dagger c_{i\beta\sigma} c_{i\beta\sigma}^\dagger c_{i\alpha\sigma} - c_{i\alpha\sigma}^\dagger c_{i\beta\sigma} c_{i\alpha\sigma}^\dagger c_{i\beta\sigma}) \} \end{aligned} \quad (3)$$

H_{int} is the centrosymmetric representation²⁰ of the multi-orbital Hubbard-Kanamori interaction²¹ that is treated at the mean field level to calculate the magnetic phase diagram, and at the RPA level to calculate the dynamical spin-susceptibility in the normal state. U is the intra-orbital repulsion, and J is the Hund's coupling parameter. The first principles calculations are performed with full potential linear augmented plane waves plus local orbitals and the local density approximation implemented in the WIEN2k²² ecosystem. The total energy was converged to 0.1 meV on a 5000 kpoint grid with an RKmax of 5. Projection onto Wannier states including

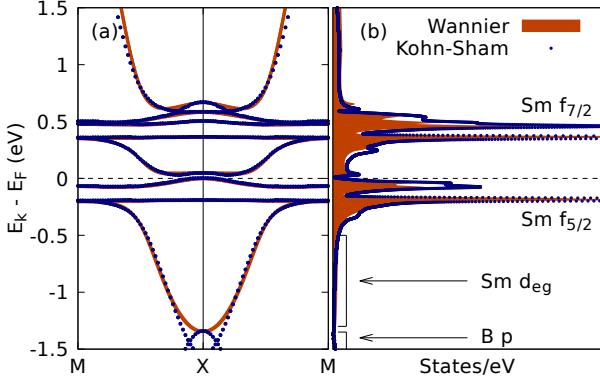


FIG. 1. Electronic structure plots contrasting LDA and Wannier projection. (a) bandstructure (b) density of states

fourth nearest neighbors is accomplished with the Wannier90 package²³, resulting in 40,500 complex hopping parameters.

Figure 1 overlays the Wannier interpolated electronic structure with the Kohn-Sham result. The density of states shows the sharp Sm f peaks with the doubly split $J = 5/2$ and triply split $J = 7/2$ multiplets just below and above the Fermi level respectively¹⁸. This electronic structure is representative of O_h point group symmetry in a weak cubic field and strong spin-orbit coupling scheme²⁴, in this respect it is commensurate with the latest tunneling spectra²⁵. The itinerant Sm d - eg bands are seen to hybridize with the localized f manifold developing a 15 meV direct gap. Excellent agreement is found between the Wannier projection and Kohn-Sham result in the low energy window $E_f \pm 500$ meV. Admittedly, a parity crossing between the hybridized Samarium $4f$ band and the Boron p state at the X point lost in this Wannier projection, likely resulting in a shift of the Berry phase. However, being interested in excitation effects, this truncated basis serves as an effective representation of the low energy physics.

Mean Field Theory – Decoupling the quartic terms in the interaction is accomplished as in Refs.^{26,27} with

$$\langle c_{i\alpha\sigma}^\dagger c_{j\beta\sigma\tau} \rangle = [n_\alpha + \frac{\sigma}{2} \cos(\mathbf{q} \cdot \mathbf{r}_i) m_\alpha] \delta_{ij} \delta_{\alpha\beta} \delta_{\sigma\sigma\tau} \quad (4)$$

This leads to a momentum space mean field Hamiltonian

$$H^{MF} = H_t + \sum_{\mathbf{p}\alpha\sigma} \theta_\alpha c_{\mathbf{p}\alpha\sigma}^\dagger c_{\mathbf{p}\alpha\sigma} + \zeta + \sum_{\mathbf{p}\alpha\sigma} \eta_{\alpha\sigma} (c_{\mathbf{p}\alpha\sigma}^\dagger c_{\mathbf{p}+\mathbf{q}\alpha\sigma} + h.c) \quad (5)$$

with mean field potentials

$$\begin{aligned} \theta_\alpha &= U n_\alpha + (2U - 5J) \sum_{\beta \neq \alpha} n_\beta \\ \eta_{\alpha\sigma} &= -\frac{\sigma}{2} (U m_\alpha + J \sum_{\beta \neq \alpha} m_\beta) \end{aligned} \quad (6)$$

and mean field constant

$$\begin{aligned} \zeta &= \frac{J}{2} \sum_{\alpha \neq \beta} m_\alpha m_\beta - U \sum_{\alpha} (n_\alpha^2 - \frac{1}{4} m_\alpha^2) \\ &\quad - (2U - 5J) \sum_{\alpha \neq \beta} n_\alpha n_\beta \end{aligned} \quad (7)$$

Calculating the phase diagram proceeds by self-consistently determining the mean field parameters n_α and $m_\alpha = n_{\alpha\uparrow} - n_{\alpha\downarrow}$, with convergence characterized by $\|D\| < 1 \times 10^{-5}$.

$$D = \langle n_{i+1}^\alpha - n_i^\alpha | \langle m_{i+1}^\alpha - m_i^\alpha | \quad (8)$$

Minimization of the norm of D gives the self-consistent condition, automatically ensuring a minimum in the free energy²⁸. The self-consistent process is repeated across different magnetic phases and ordering wavevectors. We consider a set of 5 phases characterized by 3 antiferromagnetic ordering wavevectors $\mathbf{q}_1 = (\frac{1}{2}, 0, 0)$, $\mathbf{q}_2 = (\frac{1}{2}, \frac{1}{2}, 0)$, $\mathbf{q}_3 = (\frac{1}{2}, \frac{1}{2}, \frac{1}{2})$, and the paramagnetic and ferromagnetic phases. The total particle number is constrained to the experimental average Sm valence of 2.54²⁹ during each of the self-consistency cycles.

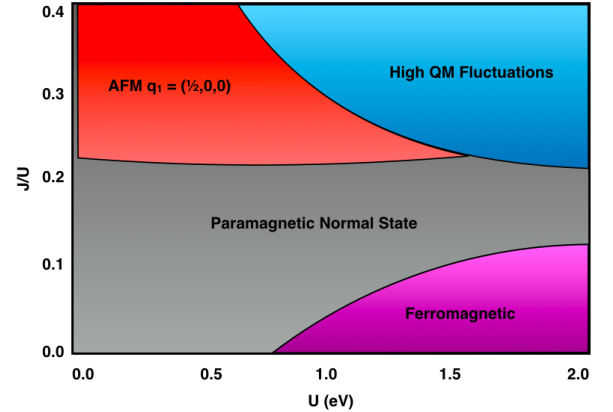


FIG. 2. Schematic magnetic phase diagram of SmB₆ obtained by mean-field treatment of first principles Wannier projection.

Figure 2 shows the zero temperature magnetic phase diagram in the plane of the interaction parameters U and J . A central feature consistent with μSR experiments³⁰ is the large paramagnetic belt found in the region with moderate correlations where the intra-orbital repulsion is comparable to the f level bandwidth W . Interestingly, in the regime of large Hund's coupling J compared to intra-orbital repulsion U , $\mathbf{q}_1 = (\frac{1}{2}, 0, 0)$ antiferromagnetic order is found to be the groundstate. We notice that high pressure experiments³¹ have already seen evidence for this 1-D like antiferromagnetic order, and a recent theoretical study reported in Ref.³² has obtained similar results. The region of $U > 1\text{eV}$, $J/U > 1/5$ shows several phases very close in energy, suggesting the

dominance of quantum fluctuations and highly competing order. For $U \gg J/U$, ferromagnetism is found to be the lowest-energy magnetic phase. It is worth mentioning that experimental evidence for ferromagnetic order is not conclusive. While μSR experiments³⁰ find no evidence of long range ferromagnetic order, magnetoresistance experiments³³ are suggestive of ferromagnetic puddling. In short, our mean-field calculations are commensurate with experiments in suggesting a system with various competing magnetic orders at zero temperature, implying the magnetic dynamics are complicated even in the normal state at finite temperatures.

Spin Susceptibility – In order to deepen our understanding of the spin dynamics in multi-orbital spin-orbit coupled systems, we study the magnetic excitations in the normal state with the following correlation tensor

$$\chi_{\alpha\alpha'\beta\beta'}^{\gamma\delta}(\mathbf{q}, i\omega_n) = \int_0^\beta d\tau e^{i\omega_n\tau} \langle T_\tau m_{\alpha\alpha'}^\gamma(\mathbf{q}, \tau) m_{\beta\beta'}^\delta(-\mathbf{q}, 0) \rangle \quad (9)$$

where for example

$$m_{\alpha\alpha'}^z(\mathbf{q}, \tau) = \sum_{\mathbf{p}\sigma} \sigma c_{\mathbf{p}+\mathbf{q}\alpha\sigma}^\dagger(\tau) c_{\mathbf{p}\alpha'\sigma}(\tau) \quad (10)$$

The lower greek indices represent orbitals and the upper indices represent magnetization direction components. Evaluation of the correlation tensor follows textbook procedures³⁴, and the bare susceptibility can be expressed by the generalized Lindhard function

$$\begin{aligned} \chi_{\bar{\alpha}\bar{\beta}}^{zz}(\mathbf{q}, \omega) &= \frac{1}{2N} \sum_{\mathbf{p}\sigma} \sigma \Xi_{\bar{\alpha}\bar{\beta}}^{ab\sigma}(\mathbf{p}, \mathbf{q}) \Lambda_{ab}(\mathbf{p}, \mathbf{q}, \omega) \\ \Xi_{\bar{\alpha}\bar{\beta}}^{ab\sigma}(\mathbf{p}, \mathbf{q}) &\equiv (U_{\alpha a\sigma}^{\mathbf{p}+\mathbf{q}})^* U_{\alpha' b\sigma}^{\mathbf{p}} (U_{\beta b\sigma}^{\mathbf{p}})^* U_{\beta' a\sigma}^{\mathbf{p}+\mathbf{q}} \\ \Lambda_{ab}(\mathbf{p}, \mathbf{q}, \omega) &\equiv \frac{n_F(\xi_{\mathbf{p}+\mathbf{q}a}) - n_F(\xi_{\mathbf{p}b})}{\omega + i\eta + \xi_{\mathbf{p}b} - \xi_{\mathbf{p}+\mathbf{q}a}} \end{aligned} \quad (11)$$

where contravariant indices are eigenbasis indices and are summed over, Ξ is the orbital projection weight, and Λ gives the thermal occupations³⁵. Here the rank four tensor is operated as a matrix by defining the sets $\bar{\alpha} = \{\alpha, \alpha'\}$ and $\bar{\beta} = \{\beta, \beta'\}$. Due to the presence of strong spin-orbit coupling, the longitudinal (χ^{zz}) and transverse (χ^\pm) functions are calculated separately since they could be different. Within the GRPA, the renormalized correlation functions become

$$\begin{aligned} \chi_{\bar{\alpha}\bar{\beta}}^{zz} &= \chi^1 + \chi^4 - \chi^2 - \chi^3 \\ \chi_{\bar{\alpha}\bar{\beta}}^\pm &= \chi^5 \end{aligned} \quad (12)$$

The functions χ^{1-5} , along with the interaction kernel are worked out in great detail in Refs.^{36,37}. The spectral function of this correlator is directly measured by INS experiments, and what is known from experiment is the low energy peaks around 14 meV cannot be attributed to phonon, crystal field, or pure magnon modes¹⁴.

Discussion – To gain insight into the origin of these peaks, we analyze the orbital components of the spectra

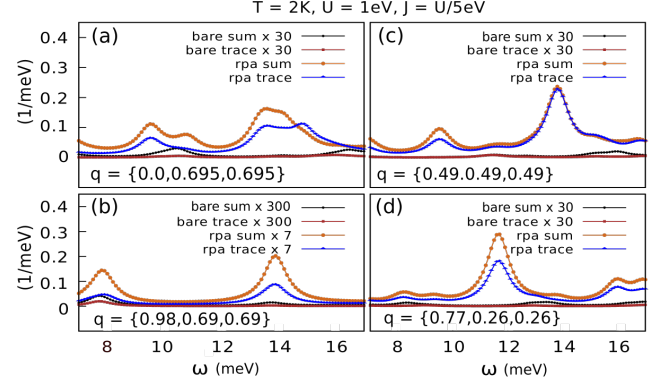


FIG. 3. Longitudinal spin response spectrum for selected scattering vectors of INS data of Ref.¹⁴. Note the spectra have been scaled differently.

TABLE I.

Function	Orbital conservation
$\sum_{\bar{\alpha}\bar{\beta}} (\chi_{\bar{\alpha}\bar{\beta}}^\pm)$	No
$\sum_{\bar{\alpha}\bar{\beta}} (\chi_{\bar{\alpha}\bar{\beta}}^{zz})$	No
$\text{tr}(\chi_{\bar{\alpha}\bar{\beta}}^\pm)$	Yes
$\text{tr}(\chi_{\bar{\alpha}\bar{\beta}}^{zz})$	Yes

around 14 meV for a set of scattering vectors tested by Ref.¹⁴. The GRPA calculations were performed on an 8000 k -point grid in the full Brillouin zone with a thermal broadening factor fixed to $\eta = 0.5$ meV.

Table I summarizes how the correlation tensor is used to classify processes depending on initial and final orbital states, and figure 3 shows two orbital decompositions of the spectral function extracted via the sum and the trace of the longitudinal function from Eqn 12. Consider first the bare and the GRPA susceptibilities in figure 3a. The bare function shows no signature at 14 meV whereas the GRPA produces peaks matching the INS data, indicating these modes are a result of electron correlations instead of wavevector nestings. Furthermore, the difference between the sum and the trace of the spectral function demonstrates the extent to which spin excitations at that wavevector have considerable orbital content. This is readily visible in comparing figure 3a, 3b, and 3d to figure 3c. If the sum and the trace have nearly identical line-shapes, the corresponding peak is mainly associated with spin-flip processes within intra-orbital channels. In this case, orbital fluctuations are not coupled to this spin mode despite the strong spin-orbit interaction. On the other hand, if the trace is only a portion of the the sum around an INS peak, the corresponding peak carries significant weight in the inter-orbital channel, and orbital fluctuations are strongly entangled with this spin excitation. Comparing the spin-spin correlation function at all four momenta plotted in figure 3, we find that the magnetic excitations at $q = (0, 0.695, 0.695)$,

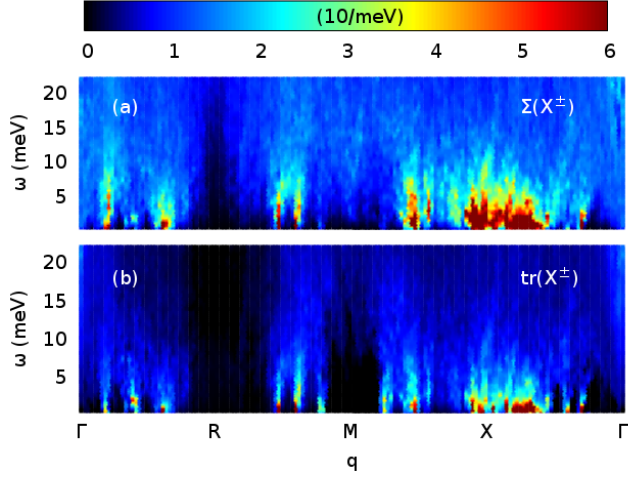


FIG. 4. (top) The sum of the transverse function for $T = 1\text{K}$, $U = 1\text{eV}$, $J = U/10$. (bottom) trace of the transverse function for $T = 1\text{K}$, $U = 1\text{eV}$, $J = U/10$.

(0.98, 0.69, 0.69) and (0.77, 0.26, 0.26) have large inter-orbital contributions while those at $q = (0.49, 0.49, 0.49)$ are mainly in the intra-orbital channels. This observation indicates that the effects of the interactions driving the spin collective modes near 14 meV are inhomogeneous throughout the momentum space, despite the fact that SmB_6 has a centrosymmetric crystal structure and the Sm point group should be at lowest D_{4h} . This strongly suggests the orbital degree of freedom plays a crucial role in the collective excitations emerging from electron correlations, and may lead to the symmetry breaking magnetic response witnessed in Ref.³⁸ for example.

Figure 4 maps the transverse spin excitation in frequency-momentum space. The inter- vs intra-orbital channels can be seen to have different structure and intensity as a function of scattering wavevector. This reiterates a strong inhomogeneity in the spin-orbital coupling, and supports the idea that the low energy states are selectively susceptible to orbital excitations. The peak around $q = X$ observed in INS and in our data can be directly tied to the phase diagram, as this excitation is associated with 1D AFM order. The lowest lying excitations exhibiting a reduced dimensionality profile has ramifications on transport properties as discussed by Ref.¹⁷, especially given the centrosymmetry present in the crystal structure and our interaction kernel. The fact that we find the X point susceptibility peaking near 4 meV is indicative that in our model, the cost of the 1D AFM excitation is within 10 meV of experiment. Given the fact we are in a weak coupling regime, this suggests that even though this is correlation driven physics, the $U \rightarrow \infty$ limit is not absolutely necessary. This alleviates chemical potential pinning and integer occupancy constraints imposed by slave bosonization for example, and is another benefit of this approach to mixed valent system. To explore this further, the onset of the excitation

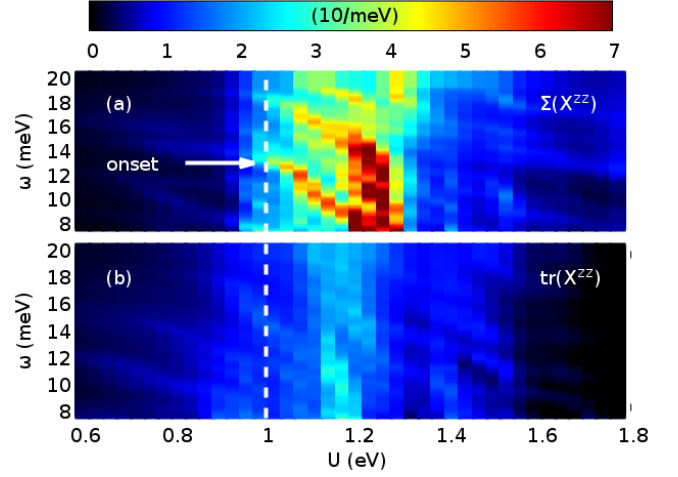


FIG. 5. Scattering at $q = (0, 0.695, 0.695)$ as a function of interaction for $T = 2\text{K}$, $J = U/5$. (a) The sum of the longitudinal function. (b) trace of the longitudinal function.

is studied as a function of local correlations.

Figure 5 shows the longitudinal susceptibility as a function of U with $J = U/5$ for the selected scattering vector $q = (0, 0.695, 0.695)$. We find that the excitation at 14 meV onsets as $U \approx W \approx 1\text{eV}$, and is driven down in energy as a function of U . While the result agrees with the previous study^{15,16}, our results further ascribe significant orbital angular momentum to the spectral weight of the 14 meV mode by comparing the trace and the sum. The trace in figure 5b showing a significantly weaker excitation profile than the sum in 5a, again shows that at this specific wavevector there is significant orbital character in the excitation. In light of the phase diagram in figure 2, increasing U drives the system into a region of high fluctuations, reducing the energy cost of instantiating this specific spin-orbital excitation. The fact that the 14 meV peak arises when $U \approx W$ places a strong constraint on theoretical treatment of correlations in SmB_6 , further showing the $U \rightarrow \infty$ limit is an unnecessary assumption if starting with an accurate electronic dispersion.

Conclusion – We have shown that a first principles model can reproduce the low energy physics in SmB_6 , and that momentum dependent entanglement between the spin and orbital degree of freedom emerges naturally from strong spin-orbit coupling. The various competing magnetic phases at zero temperature lead to non-trivial magnetic dynamics in the normal state, and spectral decomposition of the spin susceptibility exposes the anisotropic orbital character of the excitations. This first principles approach clarifies a number of intriguing features observed in the inelastic neutron scattering measurement. With the evidence presented here, we propose the orbitally degenerate non-dispersive f manifold is the perfect environment to harbor *orbital exciton* modes, a new correlation driven mode carrying exclusively orbital

angular momentum. This conjecture proffers a new physical interpretation when considering non-trivial topology with a charge-neutral Fermi surface, and provides a simple mechanism for bulk SmB_6 to couple selectively to magnetic perturbations while simultaneously ignoring the charge sector. This completely unique exciton form allows an additional pathway for low temperature specific heat anomalies, and will additionally cause an orbital dichroic signal in optical probes. Further work to address the role of topology, as well as quantitative descriptions of these contemporary exciton modes is underway.

ACKNOWLEDGMENTS

Acknowledgments – This work utilized the Extreme Science and Engineering Discovery Environment (XSEDE) supported by National Science Foundation grant number ACI-1548562. It was also supported by a Binghamton University start up fund. The authors thank Pegor Aynajian for discussions regarding INS and Feliciano Giustino for discussions regarding DFT.

-
- * email at: csingh5@binghamton.edu; visit webpage at: <http://www.linkedin.com/in/csingh5binghamton/>
- † email at: wlee@binghamton.edu; visit webpage at: <http://bingweb.binghamton.edu/~wlee/>
- ¹ A. Menth, E. Buehler, and T. H. Geballe, *Phys. Rev. Lett.* **22**, 295 (1969).
 - ² L. Kouwenhoven and L. Glazman, (2001), [arXiv:cond-mat/0104100](https://arxiv.org/abs/cond-mat/0104100).
 - ³ M. C. Hatnean, M. R. Lees, D. M. Paul, and G. Balakrishnan, *Scientific Reports* **3**, 3071 (2013).
 - ⁴ M. Dzero, K. Sun, V. Galitski, and P. Coleman, *Phys. Rev. Lett.* **104**, 106408 (2010).
 - ⁵ S. Wolgast, C. Kurdak, K. Sun, J. W. Allen, D.-J. Kim, and Z. Fisk, *Phys. Rev. B* **88**, 180405 (2013).
 - ⁶ D. Kim, S. Thomas, T. Grant, J. Botimer, Z. Fisk, and J. Xia, *Scientific Reports* **3** (2013).
 - ⁷ D. J. Kim, J. Xia, and Z. Fisk, *Nature Materials* **13**, 466 (2014).
 - ⁸ M. Neupane, N. Alidoust, S. Xu, T. Kondo, Y. Ishida, D.-J. Kim, C. Liu, I. Belopolski, Y. Jo, T.-R. Chang, *et al.*, *Nature Communications* **4**, 2991 (2013).
 - ⁹ N. Xu, P. Biswas, R. Dhaka, G. Landolt, S. Muff, C. Matt, X. Shi, N. Plumb, M. Radovic, E. Pomjakushina, *et al.*, *Nature Communications* **5** (2014).
 - ¹⁰ N. Wakeham, P. F. S. Rosa, Y. Q. Wang, M. Kang, Z. Fisk, F. Ronning, and J. D. Thompson, *Phys. Rev. B* **94**, 035127 (2016).
 - ¹¹ G. Li, Z. Xiang, F. Yu, T. Asaba, B. Lawson, P. Cai, C. Tinsman, A. Berkley, S. Wolgast, Y. S. Eo, D.-J. Kim, C. Kurdak, J. W. Allen, K. Sun, X. H. Chen, Y. Y. Wang, Z. Fisk, and L. Li, *Science* **346**, 1208 (2014).
 - ¹² B. Tan, Y.-T. Hsu, B. Zeng, M. C. Hatnean, N. Harrison, Z. Zhu, M. Hartstein, M. Kiourlappou, A. Srivastava, M. Johannes, *et al.*, *Science* **349**, 287 (2015).
 - ¹³ P. Nyhus, S. L. Cooper, Z. Fisk, and J. Sarrao, *Phys. Rev. B* **55**, 12488 (1997).
 - ¹⁴ P. Alekseev, J. Mignot, J. Rossat-Mignod, V. Lazukov, I. Sadikov, E. Konovalova, and Y. B. Paderno, *Journal of Physics: Condensed Matter* **7**, 289 (1995).
 - ¹⁵ W. T. Fuhrman and P. Nikolić, *Phys. Rev. B* **90**, 195144 (2014).
 - ¹⁶ W. T. Fuhrman, J. Leiner, P. Nikolić, G. E. Granroth, M. B. Stone, M. D. Lumsden, L. DeBeer-Schmitt, P. A. Alekseev, J.-M. Mignot, S. M. Koohpayeh, P. Cottingham, W. A. Phelan, L. Schoop, T. M. McQueen, and C. Broholm, *Phys. Rev. Lett.* **114**, 036401 (2015).
 - ¹⁷ J. Knolle and N. R. Cooper, *Phys. Rev. Lett.* **118**, 096604 (2017).
 - ¹⁸ C.-J. Kang, J. Kim, K. Kim, J. Kang, J. D. Denlinger, and B. I. Min, *Journal of the Physical Society of Japan* **84**, 024722 (2015).
 - ¹⁹ A. Yanase and H. Harima, *Progress of Theoretical Physics Supplement* **108**, 19 (1992).
 - ²⁰ The centrosymmetric approximation is used for simplicity, but some recent evidence³⁸ suggests that a more detailed treatment of the inter-orbital interaction may be pertinent.
 - ²¹ J. Kanamori, *Progress of Theoretical Physics* **30**, 275 (1963).
 - ²² P. Blaha, K. Schwarz, G. Madsen, D. Kvasnicka, and J. Luitz, *An augmented plane wave+ local orbitals program for calculating crystal properties* (2001).
 - ²³ A. A. Mostofi, J. R. Yates, G. Pizzi, Y.-S. Lee, I. Souza, D. Vanderbilt, and N. Marzari, *Computer Physics Communications* **185**, 2309 (2014).
 - ²⁴ M. Tinkham, *Group Theory and Quantum Mechanics* (Courier Corporation, 2003) p. 79.
 - ²⁵ Z. Sun, A. Maldonado, W. S. Paz, D. S. Inosov, A. P. Schnyder, J. J. Palacios, N. Y. Shitsevalova, V. B. Filippov, and P. Wahl, (2018), [arXiv:1803.08776](https://arxiv.org/abs/1803.08776).
 - ²⁶ T. Nomura and K. Yamada, *Journal of the Physical Society of Japan* **69**, 1856 (2000).
 - ²⁷ E. Dagotto, A. Moreo, A. Nicholson, Q. Luo, S. Liang, and X. Zhang, *Frontiers of Physics* **6**, 379 (2011).
 - ²⁸ D. D. Johnson, *Phys. Rev. B* **38**, 12807 (1988).
 - ²⁹ Y. Utsumi, D. Kasinathan, K.-T. Ko, S. Agrestini, M. W. Haverkort, S. Wirth, Y.-H. Wu, K.-D. Tsuei, D.-J. Kim, Z. Fisk, A. Tanaka, P. Thalmeier, and L. H. Tjeng, *Phys. Rev. B* **96**, 155130 (2017).
 - ³⁰ P. K. Biswas, Z. Salman, T. Neupert, E. Morenzoni, E. Pomjakushina, F. von Rohr, K. Conder, G. Balakrishnan, M. C. Hatnean, M. R. Lees, D. M. Paul, A. Schilling, C. Baines, H. Luetkens, R. Khasanov, and A. Amato, *Phys. Rev. B* **89**, 161107 (2014).
 - ³¹ A. Barla, J. Derr, J. P. Sanchez, B. Salce, G. Lapertot, B. P. Doyle, R. Rüffer, R. Lengsdorf, M. M. Abd-Elmeguid, and J. Flouquet, *Phys. Rev. Lett.* **94**, 166401 (2005).
 - ³² K.-W. Chang and P.-J. Chen, *Phys. Rev. B* **97**, 195145 (2018).
 - ³³ Y. Nakajima, P. Syers, X. Wang, R. Wang, and J. Paglione, *Nature Physics* **12**, 213 (2016).
 - ³⁴ G. D. Mahan, *Many-Particle Physics* (Springer Science & Business Media, 2013).
 - ³⁵ See appendix for definitions.
 - ³⁶ X. Wu, F. Yang, C. Le, H. Fan, and J. Hu, *Physical Review*

- [B 92, 104511 \(2015\)](#).
- ³⁷ S. Mukherjee and W.-C. Lee, [Physical Review B 94, 064407 \(2016\)](#).
- ³⁸ Z. Xiang, B. Lawson, T. Asaba, C. Tinsman, L. Chen, C. Shang, X. H. Chen, and L. Li, [Phys. Rev. X 7, 031054 \(2017\)](#).